

Estimating solar-radiation environment extremes

Konstantin Herbst^{1,2,*} and Athanasios Papaioannou^{3,*}

¹ Centre for Planetary Habitability (PHAB), Faculty of Mathematics and Natural Sciences, Department of Geosciences, University of Oslo, Sem Sælands vei 2A Blindern, Norway

² Institut für Planetenforschung (PF), Deutsches Zentrum für Luft- und Raumfahrt (DLR), Rutherfordstr. 2, 12489 Berlin, Germany

³ Institute for Astronomy, Astrophysics, Space Applications and Remote Sensing (IAASARS), National Observatory of Athens, I. Metaxa & Vas. Pavlou St., 15236 Penteli, Greece

Received 3 September 2024 / Accepted 8 February 2025

ABSTRACT

Context. Extreme solar particle events (ESPEs) were identified almost a decade ago, providing context for super events unleashed by our host star, the Sun. Their assumed solar origin drives the question of their “worst-case” impact, which could be profound, multifaceted, and devastating for our technological society.

Aims. Recently, we proposed a methodology that directly relates the soft X-ray flux (F_{SXR}) of the driving solar flare of a solar energetic particle (SEP) event to its “worst-case” integral fluence spectrum. In this study, we aim to put the letter to the stress test.

Methods. In this study, we employed our previous method to the ESPEs that have been confirmed in cosmogenic radionuclide records to date, retrieved their “worst-case integral spectrum, and compared the latter to the actual – independently obtained – recent reconstructions based on the radionuclide records.

Results. It is shown that our previous method makes it possible to estimate the integral fluence spectra of one of the paleo events, that is, AD774/775, one of the strongest ESPEs found within the cosmogenic radionuclide records so far. We implemented a mean ESPE utilizing four confirmed paleo ESPEs (i.e., AD993/994, AD774/775, 660 BCE, and 7176 BCE) and tested the resulting spectrum against the estimated one. Finally, we tested the same methodology for a series of strong SEP events recorded on the Earth’s surface as ground level enhancement (GLE) events. In all investigated cases, a recent re-calibration of the GOES 1–8 F_{SXR} values is considered.

Conclusions. It is shown that the proposed methodology can adequately estimate the “worst-case” integral fluence spectrum for both strong SEP events and ESPEs, quantifying their impact up to an integral energy of $\sim E > 1$ GeV.

Key words. Sun: coronal mass ejections (CMEs) – Sun: flares – Sun: particle emission – solar-terrestrial relations – Earth

1. Introduction

Solar energetic particle (SEP) events represent one of the most dynamic and impactful phenomena in space physics (Reames 2023). These events occur when particles – primarily protons, electrons, and heavier ions – are accelerated to near-relativistic speeds by solar processes (Reames 1999). As a result, the energies of SEP events span from a few kiloelectron volts to a few gigaelectron volts (see discussion in Papaioannou et al. 2023). The relativistic high-energy tail of SEPs is occupied by ground level enhancement (GLEs) events; in these events, particles are energetic enough ($E \geq 300$ MeV; see details in Mishev & Poluianov 2021), allowing them to penetrate Earth’s magnetic field and reach the lower atmosphere, producing secondary particles detectable on the ground, usually by neutron monitors (see a recent review in Papaioannou 2023). Two primary mechanisms drive SEP events: solar flares and coronal mass ejections (CMEs; e.g., Klein & Dalla 2017). On the one hand, solar flares, which are intense bursts of radiation emanating from the release of magnetic energy in the Sun’s atmosphere, can accelerate particles through magnetic-reconnection processes (Aschwanden 2002). On the other hand, CMEs involve large expulsions of plasma and magnetic field from the Sun’s corona into interplanetary space (Howard et al. 2023). The interaction of these masses expelled from the Sun with the underlying ever-present solar wind creates shockwaves that can also accelerate particles to high energies as they propagate through the

heliosphere via, for example, diffusive shock acceleration (DSA; Desai & Giacalone 2016). However, solar flares and CMEs do not evolve in isolation but rather in concert. In particular, solar flares as sudden, intense bursts of electromagnetic energy have a prominent soft-X-ray (SXR) emission. The intensity of the SXR emission often correlates with the flare’s strength. CMEs, which involve the ejection of massive amounts of solar plasma and magnetic fields into space, frequently accompany solar flares. While not all flares lead to CMEs, the most powerful flares are typically followed by significant CMEs (Yashiro et al. 2006). Both flares and CMEs are governed by the same magnetic processes in the solar atmosphere (Zhang et al. 2001; Temmer 2021). SXR emission is often an early indicator of the flare’s intensity and the likelihood of a CME (see Takahashi et al. 2016; Papaioannou et al. 2024, and references therein). Details of the SXR-CME relation can be found in Appendix A. As a result, most SEP events are associated with both of these drivers (see, e.g., Cane et al. 2010; Papaioannou et al. 2016).

Although modern GLE events (Nitta et al. 2012; Waterfall et al. 2023) are often referred to as extreme solar events, a handful of sudden, much more extreme increases have been identified in the cosmogenic radionuclide records of ^{14}C , ^{10}Be , and ^{36}Cl (e.g., Miyake et al. 2012; Mekhaldi et al. 2015). Because of the intensity of these increases, several possible explanations, including gamma-ray bursts (Hambaryan & Neuhäuser 2013) and cometary impact (Liu et al. 2014), have been discussed in the literature. Nowadays, however, we know that these spike-like increases were caused by impacting solar energetic particles (Usoskin et al.

* Corresponding authors; konstantin.herbst@geo.uio.no;
atpapaio@astro.noa.gr

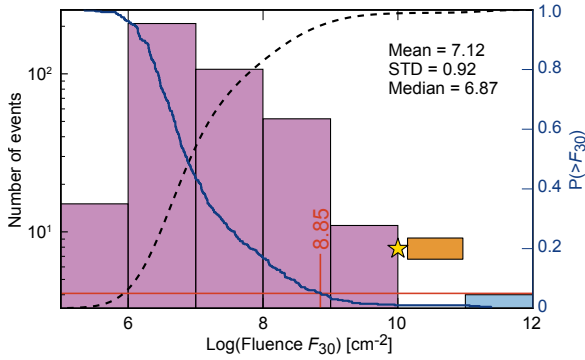


Fig. 1. Statistical distribution of F_{30} proton fluence obtained using a total of 392 SEP events recorded from 1955 to 2023 aboard spacecraft (magenta bars) and the ESPEs of the past (light blue bar). The dashed black line corresponds to the cumulative distribution function (CDF). The blue trace (right ordinate axis) corresponds to the empirical complementary CDF (CCDF) and gives the probability $P(>F_{30})$ of having an SEP event with a log fluence above a certain value F (see, e.g., Ross 2014). The horizontal red line indicates the 5% chance of exceeding the value indicated in red. The plot imprints the mean, median, and standard deviation of the entire sample for the log-fluence values. The y -axis is displayed as a log scale so that the whole range of log-fluence values can be displayed without the small ESPE values being compressed. The star corresponds to the Carrington log-fluence value of 10^{10} cm^{-2} (Cliver & Dietrich 2013). The orange rectangle depicts the lack of log-fluence values from $10^{10-11} \text{ cm}^{-2}$.

2013; Thomas et al. 2013; Cliver et al. 2014) that form the actual extreme solar particle events (ESPEs; see the detailed review by Usoskin et al. 2023). By nature, these extreme events have not been directly observed and measured. Consequently, their energy spectrum is at times represented by a scaled spectrum of the strongest ever observed hard-spectrum SEP event, GLE05, which occurred on 23 February, 1956 (see details in Papaioannou et al. 2023).

One of the first and – so far – strongest events discovered in the cosmogenic radionuclide records, the AD774/775 event, was identified in 2012 (Miyake et al. 2012) and immediately garnered a lot of attention, leading to new possibilities to investigate physical processes on the Sun (Usoskin & Kovaltsov 2021). Since then, four more ESPEs have been confirmed in all three cosmogenic radionuclide records (see details in Paleari et al. 2022; Koldobskiy et al. 2023): the 993/994 CE (Miyake et al. 2013), the 660 BCE (O’Hare et al. 2019), the 5259 BCE (O’Hare et al. 2019), and the 7176 BCE (Brehm et al. 2022)¹ event. At present, these events constitute the high-energy and low-probability tail of the SEP distribution (see, e.g., Fig. 1). With a fluence of protons at $E > 30 \text{ MeV}$ (F_{30}) estimated to be 1.5–2 orders of magnitude larger than the largest GLE on record (GLE05), the AD774/775 event is the largest SEP event described in detail so far. ESPEs are significantly larger than any SEP and/or GLE events detected since the 1950s (Koldobskiy et al. 2023), implying that such events pose an underestimated threat to our society. F_{30} can be determined from spacecraft data obtained between 1955 and 2023. In particular, a total of 392 SEP events reaching such an integral energy level have been listed to date (see details of this catalog in Papaioannou 2025). The histogram in Fig. 1 displays the distribution of the logarithm of the F_{30} values for all of these events. As can be seen, no event in the instrumental era (magenta bars)

shows an F_{30} value that exceeds the estimated Carrington event value (10^{10} cm^{-2})² (yellow star). The radionuclide-based F_{30} estimates are shown by the last bar (light blue), which represents the confirmed events discussed in Koldobskiy et al. (2023). The red horizontal line indicates the 5% chance of exceeding the value imprinted in red, indicating the tail of the distribution. It shows that only five times out of 100 may a log-fluence F_{30} larger than 8.85 (cm^{-2}) occur at our Sun. On the other hand, this means that 95 times out of 100 the log fluence will be below this value. This is further corroborated by the dotted black line, providing the CDF of the log-fluence. It indicates that the probability ($P(>F_{30})$) of the log fluence being $F_{30} \leq 8.85$ (cm^{-2}) is 0.95 (right hand ordinate; see also the discussion in Papaioannou et al. 2022). The observational gap between instrumental and paleo SEPs (orange rectangle in Fig. 1) means we cannot conclude whether these two sets of observations result from the same underlying distribution and are therefore formed by the same physical processes.

Based on the existing ^{14}C , ^{10}Be , and ^{36}Cl data, it can be hypothesized that no events larger than AD774/775 will be found in the radionuclide records from the last ten millennia (e.g., Miyake et al. 2019). However, most observed GLEs show “soft” spectra, with higher fluences of lower energy particles. Thus, previously unidentified extreme soft-spectrum events might hide in the cosmogenic radionuclide records (i.e., ^{36}Cl).

2. From soft X-rays to worst-case-scenario particle fluences

Recently, Koldobskiy et al. (2023) presented new, calibrated, multiproxy reconstructions of the integral fluence spectrum of all known ESPEs. This work provided precise, numerically derived, ready-to-use values of the reconstructed ESPE fluences $F(>E)$ (see their Table 3). At the same time, the tight connection between solar eruptive events and SEPs has been explored and discussed in numerous works (e.g., Cane et al. 2010; Papaioannou et al. 2016; Desai & Giacalone 2016).

Most recently, a method that allows the inference of the “worst-case” fluence spectrum of an SEP event solely utilizing the magnitude of the associated solar flare in terms of soft X-rays (SXR) has been proposed by Papaioannou et al. (2023). The worst-case fluence is derived from the upper limit estimation of each fluence value at each integral energy of interest, following the methodology detailed in Papaioannou et al. (2023). The latter is based on upper-limit scaling relations that convert the SXR flux to peak proton flux ($I_P(>E)$) and fluence ($F_P(>E)$) for a set of integral energies from $E > 10 \text{ MeV}$ to $E > 100 \text{ MeV}$. In particular, these authors utilized a carefully selected sample of 65 SEP events that extended from >10 to $>100 \text{ MeV}$ and identified scaling laws of SEPs to SXRs for each integral energy (i.e., >10 , >30 , >60 , and $>100 \text{ MeV}$). In addition, they converted the peak proton fluxes to fluences for each of the integral energies. An inverse power-law fit is assumed to fit the resulting SEP fluences from >10 to $>100 \text{ MeV}$. Once established, this is extended to higher integral energies (i.e., $E > 200 \text{ MeV}$ and $E > 430 \text{ MeV}$). Papaioannou et al. (2023) found that $F_P(>E)$ scales with the SXR flux as $F_{\text{SXR}}^{5/6}$. Thus, the integral fluence spectrum can be estimated directly when the F_{SXR} is known.

Table 3 of Koldobskiy et al. (2023) provides the integral fluences $F_P(>30)$, $F_P(>60)$, $F_P(>100)$, $F_P(>200)$, $F_P(>300)$, $F_P(>600)$, and $F_P(>1000)$ for the ESPEs recorded around AD993/994, AD774/775, 660 BCE, and 7176 BCE. Thus, the

¹ We note that the atmospheric ^{14}C increases of the 7176 BCE event are comparable to the ones of the AD774/775 event (see Tab.1 in Brehm et al. 2022).

² See Cliver & Dietrich (2013).

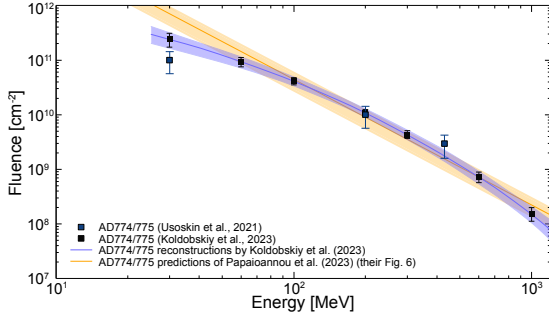


Fig. 2. Integral fluence spectra of AD774/775 event. Blue and black filled squares display the estimations based on the cosmogenic radionuclide data (Usoskin et al. 2021; Koldobskiy et al. 2023, respectively). While the magenta ribbon reflects the spectrum derived by Koldobskiy et al. (2023), the orange ribbon is obtained as a worst-case upper-limit integral-fluence spectrum based on an X600 solar flare by employing the method outlined in Papaioannou et al. (2023).

combination of these integral fluences for each integral energy leads to a well-specified range of values per energy bin. In turn, these estimates can be used to construct the upper and lower limits of the integral fluence as a function of integral energy as deduced by measurements (proxies) alone.

In the case of the AD774/775 event, Cliver et al. (2022) identified the associated SXR flux as $X400 \pm 200$ (see also Papaioannou et al. 2023; Hudson et al. 2024). This SXR flux was identified as follows: Cliver et al. (2020, i.e., their Fig. 7) began with a reduced-major-axis (RMA) fit to a scatter plot of modeled >200 MeV fluences taken from Raukunen et al. (2018) for hard-spectrum GLEs versus the peak intensities of their associated SXR flares. They then added two points for the 1956 GLE based on the estimated range of the peak SXR intensity (X10-X30) of its associated flare (as inferred from white-light and radio observations) and its >200 MeV fluence (Usoskin et al. 2020). Through these points, they extrapolated lines parallel to the RMA fit to the modeled >200 MeV fluence for the AD774 SEP event to obtain an estimate of $X285 \pm 140$ for the AD774 flare. Re-scaling the SXRs according to Hudson et al. (2024) shifts the SXR of AD774 from $X285 \pm 140$ to $X400 \pm 200$. It follows that the worst-case upper-limit SXR flux is X600. With the help of the method described in Papaioannou et al. (2023), therefore, we obtained the worst-case integral fluence spectra utilizing the X600 F_{SXR} (solid orange line embedded in an envelope depicting the $1-\sigma$ error; parameters of the fit are available in Table 3 of Papaioannou et al. 2023). As shown in Fig. 2, the so-derived spectrum and the independently obtained range of integral fluence values from Koldobskiy et al. (2023) and Usoskin et al. (2021) can be directly compared. As can be seen, our AD774/775 estimate aligns well with the fluence values derived by Usoskin et al. (2021) (blue symbols) and Koldobskiy et al. (2023) (black symbols). The underlying assumption of the aforementioned studies is that flares (denoted by their SXR measurements) drive SEPs. However, the lack of a universal correlation between spectral hardness and SXRs under a flare-only acceleration model (see, e.g., Trotter et al. 2015) suggests the need for an additional mechanism such as CME-driven shocks, thus supporting a dual-mechanism model (Papaioannou et al. 2016; Desai & Giacalone 2016). Considering the differences, the obtained alignment is promising. The spectral shape derived by Koldobskiy et al. (2023) is highlighted in purple. Given the fact that the AD774/775 event is the strongest ESPE event identified to date, it represents an upper-limit worst-case event, demonstrating what our host star, the Sun, is capable of producing

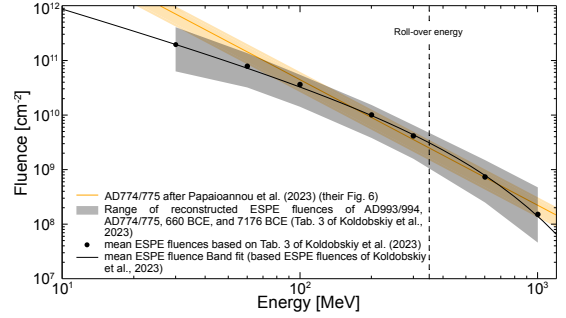


Fig. 3. Integral fluence spectra of AD774/775 event taking into account the reconstructed ESPE events around AD993/994, AD774/775, 660 BCE, and 1776 BCE. Here, the gray shade represents the spread of integral fluence values presented in Koldobskiy et al. (2023), while the filled circles show the integral energy-dependent mean of each fluence bin and the solid black line represents the corresponding band fit. The solid orange line and envelope are similar to those of Fig. 2.

(Papaioannou et al. 2023). The study of Koldobskiy et al. (2023) provides the scaled spectrum of the AD774/775 event with a $1-\sigma$ spread. This is incorporated in the direct comparison of Fig. 2. Although there is an apparent roll-over energy for ESPEs (here at $E > 300$ MeV), our simple inverse power-law representation (within the errors) gives a quite practical representation between $E > 60$ MeV and $E > 1$ GeV. Nonetheless, the spectral shape employed (i.e., inverse power-law) is restrictive for both the softening of the higher energies and the underestimation of the lower energies. As a result, while a realistic spectrum for SEPs is expected to be a double power or have an exponential rollover (see details in Appendix B), here we consider a single power-law approximation in the energy range of $E > 10$ MeV to $E > 100$ MeV, extrapolated to $E > 1$ GeV (see also the relevant discussion in Papaioannou et al. 2023). Nonetheless, in this work, it was made evident that the simple PL can provide a reasonable estimation of the fluence spectra from $E > 60$ MeV to $E > 1$ GeV, which in turn provides a quick and practical representation of the worst-case conditions. Figure 3 shows the range of the reconstructed ESPE integral fluence values per integral energy of AD993/994, AD774/775, 660 BCE, and 7176 BCE (gray shaded area, based on Koldobskiy et al. 2023). This was constructed using the four values (of the four events) for each integral energy and identifying the range of fluence values per integral energy (represented by the gray area in Fig. 3). Each vertical column led to a mean value per integral energy. The black dots represent these values. We note that the upper limit is formed by the 660 BCE event ($E < 15$ MeV) and the 7176 BCE event ($E > 15$ MeV), while the AD993/994 event forms the lower limit at all energy values. To derive an estimation of the mean of the range of integral fluences per integral energy, we utilized the band-fit function, which is a double power-law with an energy-dependent rollover (e.g., Band et al. 1993). Here, the omnidirectional event-integrated integral fluences $J(>R)$ [cm^{-2}] are given by

$$F(>R) = \begin{cases} J_0 \left(\frac{R}{1 \text{ GV}} \right)^{-\gamma_1} \exp\left(-\frac{R}{R_0}\right) & R \leq (\gamma_2 - \gamma_1)R_0 \\ J_0 \left(\frac{R}{1 \text{ GV}} \right)^{-\gamma_1} \exp\left(-\frac{R}{R_0}\right) \left(\frac{R}{R_1} \right)^{-\gamma_2} & R > (\gamma_2 - \gamma_1)R_0, \end{cases} \quad (1)$$

where J_0 represents the fluence normalization coefficient and γ_1 and γ_2 represent the low and high-rigidity power-law indices (e.g., Raukunen et al. 2018), respectively. Accordingly, the event-integrated differential spectrum (in units of $[1/(\text{cm}^2 \text{ sr GeV})]$) can be derived by

$$F(>E) = \begin{cases} \frac{1}{4\pi} J_0 \left(\frac{R}{1 \text{ GV}} \right)^{-\gamma_1} \exp\left(-\frac{R}{R_0}\right) \frac{(\gamma_1 R_0 + R)(E + E_0)}{R_0 R^2} & R \leq (\gamma_2 - \gamma_1)R_0 \\ \frac{1}{4\pi} J_0 \cdot A \cdot \gamma_2 \cdot R^{-\gamma_2} \frac{E + E_0}{R^2} & R > (\gamma_2 - \gamma_1)R_0. \end{cases} \quad (2)$$

Table 1. Quantities of GLEs presented in Fig. 4.

$E > \text{MeV}$	GLE55 $F [\text{cm}^{-2}]$	GLE56 $F [\text{cm}^{-2}]$	GLE59 $F [\text{cm}^{-2}]$	GLE60 $F [\text{cm}^{-2}]$	GLE62 $F [\text{cm}^{-2}]$	GLE63 $F [\text{cm}^{-2}]$	GLE64 $F [\text{cm}^{-2}]$	GLE65 $F [\text{cm}^{-2}]$	GLE66 $F [\text{cm}^{-2}]$	GLE67 $F [\text{cm}^{-2}]$	GLE69 $F [\text{cm}^{-2}]$	GLE70 $F [\text{cm}^{-2}]$	GLE71 $F [\text{cm}^{-2}]$
29	1.22E+08	1.61E+07	1.89E+09	1.24E+08	6.98E+08	8.02E+07	4.01E+07	2.51E+09	2.77E+08	1.31E+08	3.46E+08	1.55E+08	2.32E+07
60	4.95E+07	5.65E+06	4.68E+08	5.98E+07	1.30E+08	2.15E+07	1.29E+07	2.91E+08	9.00E+07	2.90E+07	1.59E+08	5.79E+07	7.79E+06
103	2.06E+07	2.22E+06	1.44E+08	3.08E+07	3.27E+07	6.95E+06	4.89E+06	5.92E+07	3.25E+07	8.66E+06	7.95E+07	2.10E+07	3.12E+06
196	5.09E+06	5.48E+05	2.75E+07	1.13E+07	4.92E+06	1.37E+06	1.21E+06	8.87E+06	6.92E+06	1.73E+06	2.80E+07	4.96E+06	8.65E+05
294	1.93E+06	1.93E+05	8.50E+06	5.27E+06	1.33E+06	4.45E+05	4.40E+05	2.91E+06	2.15E+06	5.91E+05	1.28E+07	1.96E+06	3.50E+05
407	8.24E+05	7.52E+04	2.76E+06	2.46E+06	3.92E+05	1.61E+05	1.65E+05	1.18E+06	6.65E+05	2.20E+05	5.88E+06	8.62E+05	1.48E+05
602	2.79E+05	2.30E+04	6.14E+05	8.04E+06	8.17E+04	4.14E+04	4.02E+04	4.14E+05	1.32E+05	6.14E+04	1.87E+06	2.96E+05	4.36E+04
1000	5.96E+04	4.44E+03	7.25E+04	1.56E+05	9.27E+03	5.31E+03	4.18E+03	1.19E+05	1.39E+04	1.04E+04	3.24E+05	6.18E+04	5.85E+03
$F_{\text{SXR}} [\text{W/m}^2]$	9.40E-04	1.10E-04	5.70E-04	1.44E-03	1.00E-04	7.10E-05	3.10E-04	1.70E-03	1.00E-03	8.30E-04	7.10E-04	3.40E-04	5.10E-05
$F_{\text{SXR,rec}} [\text{W/m}^2]$	1.34E-03	1.57E-04	8.14E-04	2.11E-03	1.43E-04	1.01E-04	4.43E-04	2.57E-03	1.55E-03	1.33E-03	1.02E-03	4.86E-04	7.29E-05

Notes. The integral fluence per $F(>E) [\text{cm}^{-2}]$ for a set of eight integral energies for 12 GLEs, as published by Koldobskiy et al. (2021). Associated solar flare flux $F_{\text{SXR}} [\text{W/m}^2]$ followed by $F_{\text{SXR,rec}} [\text{W/m}^2]$, which are the currently accurate SXR fluxes. For these values, proper scaling was applied (using a multiplicative factor of 1/0.7 for the GOES 1–8 channel). The saturated strong X-class event values for GLE60, GLE65, GLE66, GLE67, GLE69, and GLE72 also need further attention; their re-scaled SXR classes are taken from Hudson et al. (2024).

Here, $A = [(\gamma_2 - \gamma_1)R_0]^{(\gamma_2 - \gamma_1)} \exp(\gamma_1 - \gamma_2)$ and E_0 is the rest mass energy of a proton (0.938 GeV). The following parameters have been found to fit the values best (i.e., the black dots in Fig. 3): $J_0 = 8.5 \cdot 10^{13} \pm 1 \cdot 10^{11} \text{ cm}^{-2}$, $\gamma_1 = 0.65 \pm 0.02$, $\gamma_2 = 7.0 \pm 0.05$, and $R_0 = 0.35 \pm 0.01 \text{ GV}$. The corresponding rollover energy is displayed as the black dashed line.

To test whether the worst-case integral fluence spectra inferred from F_{SXR} can further be applied to modern events, we turn to the strongest SEP events that have been recorded on Earth as GLEs above the ever-present background of Galactic cosmic rays (see a recent review on the subject in Papaioannou 2023, and references therein). Therefore, the published integral fluence spectra of the GLEs between 1956 and 2017 (i.e., covering GLE55 – GLE71³) by Koldobskiy et al. (2021) were used (see Table 1 for more details).

Further, we utilized the newly re-calibrated F_{SXR} values for the saturated GOES events (Hudson et al. 2024) and scaled the rest by utilizing a multiplicative factor of 1/0.7 (see also Papaioannou et al. 2023). Table 1 provides all information on the GLEs employed and gives their initial F_{SXR} and the newly re-calibrated values ($F_{\text{SXR,rec}}$). Thereby, the lowest $F_{\text{SXR,rec}}$ value used in our estimations is $7.2 \cdot 10^{-5} \text{ W/m}^2$ (M7.2), which is associated with GLE71 on 17 May, 2012 (Richardson et al. 2014), while the highest $F_{\text{SXR,rec}}$ used is $2.57 \cdot 10^{-3} \text{ W/m}^2$ (X25.7) and is associated with GLE65. Based on these $F_{\text{SXR,rec}}$ values, a band of the worst-case integral fluence spectra is reconstructed.

The results are shown in Fig. 4 presenting the integral fluence spectra obtained for each GLE (Koldobskiy et al. 2021) combined with the range of the worst-case integral fluence spectra obtained from the method outlined in Papaioannou et al. (2023, orange band). Again, our worst-case integral fluence spectrum agrees well with the those of the GLEs between 1956 and 2017. This suggests that the method outlined in Papaioannou et al. (2023) can reliably estimate the worst-case integral fluence spectra up to $\sim E > 1 \text{ GeV}$ – taking into account the limitations of the spectral form discussed here and in Appendix B.

3. Conclusions

The extremes of solar energetic particles were revealed only a decade ago (Miyake et al. 2012) and brought a rapid change in the field since they brought many more questions than answers (see the detailed discussion in Usoskin et al. 2023). Assuming

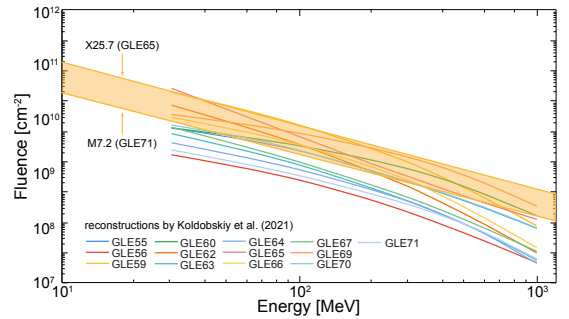


Fig. 4. Integral fluence spectrum for GLEs from 1956–2017. Each line is a band fit (see Eq. (2)) to the values presented in Table 1. The orange range depicts the worst-case estimated integral fluence spectrum for the lower and highest re-calibrated F_{SXR} values of the associated solar flares for GLE71 (lower) and GLE65 (higher). We note that the results are represented by their obtained PL fit, per case, excluding the according error estimates.

that our host star, the Sun, drives such events and that those represent a high-energy and low-probability tail of the regular SEP distribution (Usoskin & Kovaltsov 2021), it is desirable to be able to estimate their resulting worst-case integral fluence spectra to more reliably estimate the direct technological and societal consequences of such events.

We employed the methodology detailed in Papaioannou et al. (2023) and showed that it is possible to accurately estimate the integral fluence spectra of one of the strongest extreme SEP events ever observed (i.e., AD774/775, Fig. 2). The concept was further tested against a mean ESPE obtained based on four extreme SEP events found in cosmogenic radionuclide records (i.e., AD993/994, AD774/775, 660 BCE, and 7176BCE; Koldobskiy et al. 2023, see Fig. 3). It was additionally tested on a series of strong measured SEP events recorded at the surface of the Earth, i.e., GLEs (Fig. 4). Our derived worst-case integral influences seem to hold true for all cases, providing a robust upper-limit estimation for all (extreme) solar events.

AD774/775 is the only ESPE event for which a solar association, in terms of SXRs, has been possible (Cliver et al. 2022). In addition, the comparison in Fig. 4 between the mean ESPE spectrum (black line) and the derived spectrum from AD774/775 (orange line) is suggestive of the magnitude of flares that lead to ESPEs, which should be in the range of a few X100, and that the concept presented here could provide an estimate of the spectrum for ESPEs if the triggering SXR flux is known.

³ For example, <https://gle.oulu.fi/>

Our method assumes a direct scaling relation between SXR flux F_{SXR} and the obtained integral fluence $F(>E)$ (see details in Papaioannou et al. 2023). In this work, we utilized the scaled F_{SXR} flux for the first time (see details in Hudson et al. 2024). Our method does not underpin the physical processes involved in the acceleration and propagation of such extreme SEP events. Instead, it directly estimates and quantifies the effects of these changes. The verification of the concept provides valuable insight: even if we do not yet know how these extreme events are unleashed by the Sun and if these are “black swans” (produced by already known physical processes) or “red dragons” (produced by completely unknown processes; see, e.g., Cliver et al. 2022; Usoskin et al. 2023), we do know that such events will strike again, rendering our interconnected and technologically dependent society completely vulnerable.

With upcoming missions such as PLATO (Rauer et al. 2014, 2024), searching for terrestrial planets around, for example, G-type and Sun-like stars, it is essential to constrain the stellar particle- and radiation environments to be expected within the habitable zone of such systems (e.g., Engelbrecht et al. 2024; Herbst et al. 2024). Caution is needed when a scaling relation is established for a particular system and used for another. Uncertainty arises from differences in the stellar conditions compared to our Sun (e.g., temperature, density, magnetic field) and the stellar/solar wind properties that affect particle acceleration and propagation dynamics. Furthermore, the level of activity of a star versus our Sun, in terms of flare and CME occurrence, directly affects the SXR-SEP relations (see also the discussion in Papaioannou et al. 2023). Assuming the Sun to be an ordinary G-type star, our method also provides a first-order approximation of the worst-case integral stellar energetic particle fluence of an active solar twin at the exoplanetary locations, in turn paving the way for sophisticated studies of the impact cosmic rays have on exoplanetary atmospheres (i.e., climate and chemistry), transmission spectra, and biosignatures such as methane and ozone (e.g. Herbst et al. 2019; Chen et al. 2021; Herbst et al. 2024).

Acknowledgements. KH and AP acknowledge the International Space Science Institute and the supported International Team 441: *High Energy Solar Particle Events Analysis (HEROIC)* and Team 464: *The Role Of Solar And Stellar Energetic Particles On (Exo)Planetary Habitability (ETERNAL)*. KH further acknowledges the support of the DFG priority program SPP 1992 “Exploring the Diversity of Extrasolar Planets (HE 8392/1-1)”. AP acknowledges NASA/LWS project NNH19ZDA001N-LWS. This project has received funding from the Research Council of Norway through the Centres of Excellence funding scheme, project number 332523 (PHAB). Part of this work has received funding from the European Union’s Horizon Europe programme under grant agreement No 101135044 (SPEARHEAD). The research was partly funded by the European Union (ERC, PastSolarStorms, grant agreement n° 101142677). Views and opinions expressed are however those of the author(s) only and do not necessarily reflect those of the European Union or the European Research Council. Neither the European Union nor the granting authority can be held responsible for them.

References

Aschwanden, M. J. 2002, *Space Sci. Rev.*, **101**, 1
 Band, D., Matteson, J., Ford, L., et al. 1993, *ApJ*, **413**, 281
 Brehm, N., Christl, M., Knowles, T. D. J., et al. 2022, *Nat. Commun.*, **13**, 1196
 Cane, H. V., Richardson, I. G., & von Roseninge, T. T. 2010, *J. Geophys. Res. (Space Phys.)*, **115**, A08101
 Chen, H., Zhan, Z., Youngblood, A., et al. 2021, *Nat. Astron.*, **5**, 298
 Cliver, E. W., & Dietrich, W. F. 2013, *J. Space Weather Space Clim.*, **3**, A31
 Cliver, E. W., Tylka, A. J., Dietrich, W. F., & Ling, A. G. 2014, *ApJ*, **781**, 32
 Cliver, E. W., Hayakawa, H., Love, J. J., & Neidig, D. F. 2020, *ApJ*, **903**, 41
 Cliver, E. W., Schrijver, C. J., Shibata, K., & Usoskin, I. G. 2022, *Liv. Rev. Sol. Phys.*, **19**, 2
 Desai, M., & Giacalone, J. 2016, *Liv. Rev. Sol. Phys.*, **13**, 1
 Dröge, W. 2000, *ApJ*, **537**, 1073

Ellison, D. C., & Ramaty, R. 1985, *ApJ*, **298**, 400
 Engelbrecht, N. E., Herbst, K., Strauss, R. D. T., et al. 2024, *ApJ*, **964**, 89
 Gopalswamy, N. 2018, in *Extreme Events in Geospace. Origins, Predictability, and Consequences*, ed. N. Buzulukova, 37
 Hambaryan, V. V., & Neuhäuser, R. 2013, *MNRAS*, **430**, 32
 Herbst, K., Grenfell, J. L., Sinnhuber, M., et al. 2019, *A&A*, **631**, A101
 Herbst, K., Bartenschlager, A., Grenfell, J. L., et al. 2024, *ApJ*, **961**, 164
 Howard, R. A., Vourlidas, A., & Stenborg, G. 2023, *Front. Astron. Space Sci.*, **10**, 1264226
 Hudson, H., Cliver, E., White, S., et al. 2024, *Sol. Phys.*, **299**, 39
 Kiselev, V. I., Meshalkina, N. S., & Grechnev, V. V. 2022, *Sol. Phys.*, **297**, 53
 Klein, K.-L., & Dalla, S. 2017, *Space Sci. Rev.*, **212**, 1107
 Klein, K.-L., & Trotter, G. 2001, *Space Sci. Rev.*, **95**, 215
 Koldobskiy, S., Raukunen, O., Vainio, R., Kovaltsov, G. A., & Usoskin, I. 2021, *A&A*, **647**, A132
 Koldobskiy, S., Mekhaldi, F., Kovaltsov, G., & Usoskin, I. 2023, *J. Geophys. Res. (Space Phys.)*, **128**, e2022JA031186
 Kouloumvakos, A., Papaioannou, A., Waterfall, C. O. G., et al. 2024, *A&A*, **682**, A106
 Liu, Y., Zhang, Z.-F., Peng, Z.-C., et al. 2014, *Sci. Rep.*, **4**, 3728
 Masson, S., Antiochos, S. K., & DeVore, C. R. 2013, *ApJ*, **771**, 82
 Mekhaldi, F., Muscheler, R., Adolph, F., et al. 2015, *Nat. Commun.*, **6**, 1
 Mewaldt, R. A., Looper, M. D., Cohen, C. M. S., et al. 2012, *Space Sci. Rev.*, **171**, 97
 Mishev, A., & Poluianov, S. 2021, *Sol. Phys.*, **296**, 129
 Miyake, F., Nagaya, K., Masuda, K., & Nakamura, T. 2012, *Nature*, **486**, 240
 Miyake, F., Masuda, K., & Nakamura, T. 2013, *Nat. Commun.*, **4**, 1748
 Miyake, F., Usoskin, I., & Poluianov, S. eds. 2019, *Extreme Solar Particle Storms* (IOP Publishing), 2514
 Mohan, A., Gopalswamy, N., Raju, H., & Akiyama, S. 2024, *A&A*, **691**, L8
 Nitta, N. V., Liu, Y., DeRosa, M. L., & Nightingale, R. W. 2012, *Space Sci. Rev.*, **171**, 61
 O’Hare, P., Mekhaldi, F., Adolph, F., et al. 2019, *Proc. Nat. Acad. Sci.*, **116**, 5961
 Paleari, C. I., Mekhaldi, F., Adolph, F., et al. 2022, *Nat. Commun.*, **13**, 214
 Papaioannou, A. 2023, *NMDB@Athens: Proceedings of the Hybrid Symposium on Cosmic Ray Studies with Neutron Detectors, September 26-30, 2022*, **2**, 113
 Papaioannou, A. 2025, <https://zenodo.org/records/15083732>
 Papaioannou, A., Sandberg, I., Anastasiadis, A., et al. 2016, *J. Space Weather Space Clim.*, **6**, A42
 Papaioannou, A., Vainio, R., Raukunen, O., et al. 2022, *J. Space Weather Space Clim.*, **12**, 24
 Papaioannou, A., Herbst, K., Ramm, T., et al. 2023, *A&A*, **671**, A66
 Papaioannou, A., Herbst, K., Ramm, T., Lario, D., & Veronig, A. M. 2024, *A&A*, **690**, A60
 Patsourakos, S., Vourlidas, A., Török, T., et al. 2020, *Space Sci. Rev.*, **216**, 131
 Petrosian, V. 2012, *Space Sci. Rev.*, **173**, 535
 Rauer, H., Catala, C., Aerts, C., et al. 2014, *Exp. Astron.*, **38**, 249
 Rauer, H., Aerts, C., Cabrera, J., et al. 2024, arXiv e-prints [arXiv:2406.05447]
 Raukunen, O., Vainio, R., Tylka, A. J., et al. 2018, *J. Space Weather Space Clim.*, **8**, A04
 Reames, D. V. 1999, *Space Sci. Rev.*, **90**, 413
 Reames, D. V. 2023, *Front. Astron. Space Sci.*, **10**, 1254266
 Richardson, I. G., von Roseninge, T. T., Cane, H. V., et al. 2014, *Sol. Phys.*, **289**, 3059
 Ross, S. M. 2014, in *Introduction to Probability and Statistics for Engineers and Scientists (Fifth Edition)*, 5th edn. (Boston: Academic Press)
 Salas-Matamoros, C., & Klein, K. L. 2015, *Sol. Phys.*, **290**, 1337
 Takahashi, T., Mizuno, Y., & Shibata, K. 2016, *ApJ*, **833**, L8
 Temmer, M. 2021, *Liv. Rev. Sol. Phys.*, **18**, 4
 Thomas, B. C., Melott, A. L., Arkenberg, K. R., & Snyder, B. R., II 2013, *Geophys. Res. Lett.*, **40**, 1237
 Trotter, G., Samwel, S., Klein, K. L., Dudok de Wit, T., & Miteva, R. 2015, *Sol. Phys.*, **290**, 819
 Usoskin, I. G., & Kovaltsov, G. A. 2021, *Geophys. Res. Lett.*, **48**, e94848
 Usoskin, I., Kromer, B., Ludlow, F., et al. 2013, *A&A*, **552**, L3
 Usoskin, I., Koldobskiy, S., Kovaltsov, G., et al. 2020, *A&A*, **640**, A17
 Usoskin, I., Koldobskiy, S., Kovaltsov, G., et al. 2021, in *Proceedings of 37th International Cosmic Ray Conference - PoS(ICRC2021)*, 395, 1319
 Usoskin, I., Miyake, F., Baroni, M., et al. 2023, *Space Sci. Rev.*, **219**, 73
 Waterfall, C. O. G., Dalla, S., Raukunen, O., et al. 2023, *Space Weather*, **21**, e2022SW003334
 Yashiro, S., Akiyama, S., Gopalswamy, N., & Howard, R. A. 2006, *ApJ*, **650**, L143
 Zhang, J., Dere, K. P., Howard, R. A., Kundu, M. R., & White, S. M. 2001, *ApJ*, **559**, 452

Appendix A: Soft X-ray and CME relations

Observations and theoretical studies have established a significant relationship between coronal mass ejections (CMEs) and the thermal energy release traced by associated solar flare soft X-ray (SXR) emissions (Patsourakos et al. 2020). Statistical analyses indicate that most CMEs exhibit some level of X-ray emission (Yashiro et al. 2006). However, solar flares occur more frequently than CMEs, suggesting a lack of one-to-one correspondence. Nonetheless, the likelihood of a CME being associated with a flare increases with flare intensity in terms of SXR flux (see Fig. 1 of Yashiro et al. 2006).

A moderate correlation has been identified between CME speeds and the peak SXR flux of associated flares (Salas-Matamoros & Klein 2015; Takahashi et al. 2016; Papaioannou et al. 2024). This correlation arises because solar eruptive events – flares and CMEs – are interconnected, both resulting from magnetic field restructuring in the corona. However, significant scatter in the data (see e.g., Fig. 3 in Papaioannou et al. 2024) suggests that while SXR emissions relate to CME kinematics, additional factors influence CME dynamics.

Several studies have explored scaling relations between CME properties and SXRs. For instance, Takahashi et al. (2016) found that CME speed (V_{CME}) scales with the SXR photon flux (F_{SXR}) as $V_{CME} \propto F_{SXR}^{0.30 \pm 0.04}$, implying that more intense flares are generally associated with faster CMEs. Expanding on this, upper-limit scaling relations for CME speeds have been derived based on SXR emissions (Papaioannou et al. 2024) and active region (AR) energy (see e.g., Gopalswamy 2018). More recently, Mohan et al. (2024) applied the concept of scaling laws to investigate analogous correlations, extending the concept of these relations to stellar flares and CMEs.

While these scaling laws provide valuable insights into CME-SXR connections, significant variability remains. Factors such as the surrounding magnetic environment, CME geometry, and projection effects contribute to the observed scatter. Thus, although SXR measurements serve as crucial indicators of CME dynamics, they represent only one aspect of a complex interplay of solar eruptive processes (see the relevant discussion in Papaioannou et al. 2024).

Appendix B: Spectral shape

Flares and CMEs are widely recognized to almost always coincide during strong SEP events, which typically obscures the primary acceleration mechanisms (see Kiselev et al. 2022, and references therein). Thus, double power-law spectra in SEPs are expected. Such spectra are frequently observed, spanning from the lowest proton energies up to several hundred MeV (e.g. Mewaldt et al. 2012). They are commonly attributed to: (a) the presence of two distinct accelerators—such as CME-driven shocks and flare-related processes. In particular, the assumption is that CME-driven shocks are the dominant acceleration mechanism at lower energies (see, e.g. Desai & Giacalone 2016) and flare-associated processes, such as magnetic reconnection, dominate at higher energies (Klein & Trotter 2001). As a result, below the break energy, the spectrum exhibits a flatter slope (shock acceleration), while above it, the slope becomes steeper (flare-related acceleration); and (b) low-energy particles are more susceptible to scattering and energy losses due to interactions with the solar wind and interplanetary medium, including Coulomb collisions and adiabatic deceleration, which further modify their spectrum (Dröge 2000) while high-energy particles, being less

influenced by these processes, tend to retain spectral features closer to their source (Reames 1999). Nonetheless, it is also possible for a single accelerator to produce such spectra under specific conditions: (i) CME-driven shocks can produce a double power-law spectrum if the acceleration efficiency varies across different energy ranges. For instance, the presence of stronger turbulence at higher energies or a limited supply of low-energy seed particles can naturally lead to a change in the spectral slope (Ellison & Ramaty 1985); (ii) shock geometry and evolution can also affect particle acceleration. As the shock expands and weakens, it may favor acceleration at certain energy ranges over others, leading to a break in the spectrum (Kouloumvakos et al. 2024); (iii) even if the initial spectrum from a single accelerator is a pure power-law, transport effects such as scattering, energy loss, and escape from the shock region can create a double power-law signature. For example, Coulomb collisions can deplete low-energy particles, while interplanetary propagation can modify high-energy particle distributions (Dröge 2000); (iv) a single mechanism, such as stochastic acceleration (second-order Fermi processes), can inherently produce a spectrum with a break if the energy gain per interaction or the rate of particle injection into the process changes with energy (Petrosian 2012) and (v) flare-accelerated electrons and protons are injected both downward into flare loops and upward into a forming flux rope. These particles remain trapped until the expanding flux rope reconnects with an open coronal structure, releasing them into interplanetary space. Within the dense flux rope, Coulomb collisions reduce the low-energy portion of the proton spectrum. Meanwhile, the CME-driven shock independently accelerates a population of suprathermal particles present in the corona and interplanetary medium, gradually increasing their energy spectrum and replenishing the lower-energy component. Together, these processes result in a double power-law proton spectrum, characterized by a flatter slope below the break energy and a steeper slope above it (Masson et al. 2013). Thus, the spectra of low-energy and high-energy particles in SEPs are typically not aligned, reflecting their origins from possibly different acceleration processes and the subsequent propagation effects.